ChemComm

Chemical Communications

Accepted Manuscript

Volume 54
Number 1
4 January 2018
Pages 1-112

ChemComm

Chemical Communications

rsc.li/chemcomm

ISSN 1359-7345

COMMUNICATION
S. J. Connon, M. O. Senge et al
Conformational control of nonplanar free base porphyrins:
towards bifunctional catalysts of tunable basicity

COMMUNICATION

Exploration of the polymorphic solid-state landscape of an amide-linked organic cage using computation and automation

C. E. Shields,[a] T. Fellowes,[a] A. G. Slater,[a] A. I. Cooper,[a] K. G. Andrews,*[b] and F. T. Szczypiński*[a]

Organic cages can possess complex, functionalised internal cavities that make them promising candidates for synthetic enzyme mimics. Conformationally flexible but chemically robust structures are needed for adaptable guest binding and catalysis, but these rapidly exchanging systems are difficult to resolve in solution. Here, we use inexpensive calculations and high-throughput crystallisation experiments to identify accessible cage conformations for a recently reported organic cage by 'locking' them in the solid state. The conformers identified exhibit a range of distances between the carboxylic acid groups in the internal cavity, suggesting adaptability towards binding a wide array of target guest molecules. The complexity of the observed crystal structures goes beyond what is possible with state-of-the-art crystal structure prediction.

Molecules that possess permanent cavities are desirable for applications in both the solution and solid state, ranging from catalysis and sensing,[1,2] to gas storage and separation, [3,4] to permanently porous liquids.[5] In particular, covalent organic cages have attracted attention due to their solution processability, chemical tunability, and unique host-guest chemistry.[6–8] Like enzymatic receptors, organic cages can bind guests within their cavities,[9] allowing the host to act as a supramolecular protecting group or template,[10] or improving the rate or selectivity of a reaction.[2,11] Most organic cages are synthesised through dynamic covalent chemistry and are often isolated as a high-symmetry species that precipitates from solution.[12] When under thermodynamic control, such reactions must be carried out at high dilution since high concentrations can shift the equilibrium towards polymer or catenane formation. Hence, the solution-phase applications of cages formed through labile dynamic covalent chemistry are limited.[6,13]

To address the labile nature of bonding in organic cages, many groups have turned to post-synthetic modification strategies. Trapping of highly soluble symmetrical imine species by reduction to the corresponding amine prevents dynamic exchange in solution, and the resulting cages can easily be isolated by solvent removal.[14–16] Another strategy is oxidation to the amide cage.[17–19] Amide-linked organic cages are chemically stable relative to imine-linked cages, and retain their rigidity unlike amine-linked cages. Furthermore, amide moieties can act as additional interaction sites with molecules of varying polarities. Different relative orientations of the resulting amide groups lead to further stereoelectronic de-symmetrisation

from a highly symmetric cage structure.[20] Such de-symmetrisation is crucial for the strong binding of low symmetry guests, such as drug molecules and metabolites. Thus, amide cages provide a balance of flexibility and rigidity necessary for adaptive binding modes, akin to induced fit binding seen in enzymatic systems.[9,21] The synthesis of low-symmetry structures is often hampered by poor reaction yields,[22] or the need for careful precursor design and expensive high-level calcuclulations,[23–26] although some discoveries can occur serendipitously.[27] Recently, Andrews and Christensen reported multi-gram synthesis of an amide-linked organic cage **1**, using Pinnick oxidation to trap metastable imine cages *in situ* (Fig. 1, left).[19]
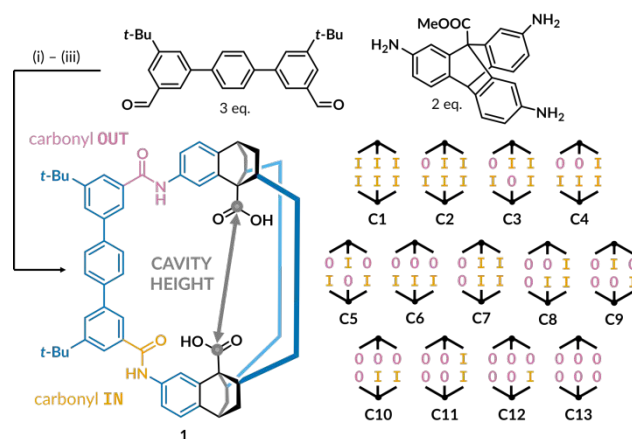

Fig. 1 Chemical structure of cage **1** and its thirteen possible amide configurations. The carbonyl group pointing outside the cavity is shown in purple and inside in orange. The cavity height is defined as the distance between the carbon atoms on the acid groups. Reaction conditions: (i) CF_3COOH, toluene/THF (4:1); (ii) $NaClO_2$, CH_3COOH, tetramethylethylene; (iii) NaOH, dioxane/water (3:1).[19]

Cage **1** is a rare example of an endohedrally-functionalised cage with two carboxylic acid groups that point into the cavity and are accessible for guest binding. Furthermore, restricted rotation around the amide bonds results in 13 unique cage conformations where the six carbonyl groups point either into or out of the cavity (Fig. 1, right). Initial crystallisation by vapour diffusion yielded conformer **C9**, but low-temperature ^{1}H NMR spectra of cage **1** in THF-d_8 show only one symmetric set of peaks, suggesting either a single symmetrical conformer (corresponding to **C1** or **C13**), or a structure that is highly fluxional on the NMR timescale.[19,20] Understanding the conformational landscape of cage **1** is important because the properties of the cavity are expected to depend on the acid-acid distance (cavity height), which depends on the relative orientations of the amide groups. Here, we set out to isolate the different conformers of cage **1** in the solid state to aid the development of amide cages towards catalysis and sensing applications.

To identify which cage conformers can be accessed

[a.] Materials Innovation Factory and Department of Chemistry, University of Liverpool, 51 Oxford Street, Liverpool, L7 3NY, UK, email: filip.szczypinski@liverpool.ac.uk
[b.] Department of Chemistry, Durham University, Lower Mount Joy, South Rd, Durham DH1 3LE, UK, email: keith.g.andrews@durham.ac.uk

COMMUNICATION   **Journal Name**

experimentally, we started with a computational analysis of the potential energy landscape. As cage **1** consists of 250 atoms connected by multiple rotatable bonds, we deemed it beyond the capabilities of the state-of-the-art crystal structure prediction methods.[31] Furthermore, we anticipated that interactions with solvent molecules would greatly affect the actual crystal packing.[32–34] Therefore, to inform our structural determination efforts, we limited our calculations to an extensive conformer search of an isolated cage structure in implicit THF solvent. The initial conformer scan using CREST with the GFN2-xTB method yielded twelve of the enumerated conformations of cage **1** within 50 kJ mol⁻¹.[35,36] Conformer **C1** was too high in energy to be identified this way, which is unsurprising given the high strain caused by all the amide carbonyls pointing towards the centre of the cavity. Resulting conformers were further optimised with a low-cost composite B97-3c method designed by Brandenburg *et al.*[37] (see ESI for the resulting structures). We then calculated single point energies for all conformations with a number of dispersion-corrected DFT functionals and basis sets (ESI, Table S4).[38]
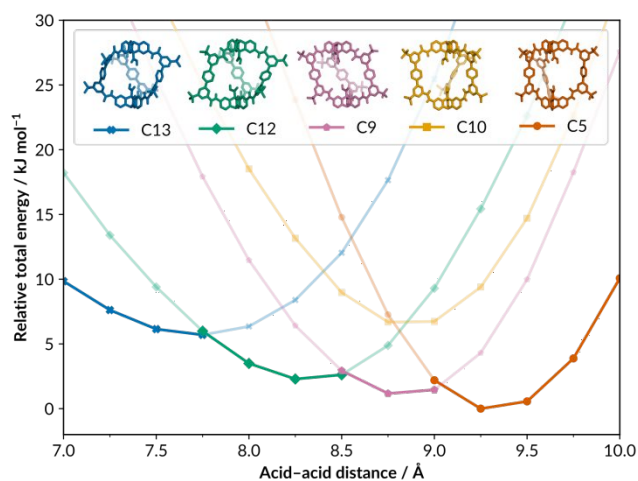

Fig. 2 Five lowest-energy identified conformers of cage **1** (optimised with B97-3c, SMD=THF) and their relaxed potential energy scans (PBE-D3(BJ)/def2-TZVP, SMD=THF).

Since our task was energy ranking of different conformers, it is perhaps unsurprising that double-zeta basis set results deviated significantly from larger basis sets (Table S4) and completeness was assumed with def2-QZVP.[39] Conformer **C9** was identified as the lowest-energy conformer with PBE,[40] PBE0,[41] and B3LYP functionals,[42] while conformer **C13** was found to be preferred in the case of M06-2X,[43] ωB97M-V,[44] and ωB97X-D3.[45] Given the observation of conformer **C9** in the previous study,[19] and substantially lower computation cost, we turned to PBE-D3(BJ)/def2-TZVP (SMD=THF) method for further analysis. Even though the energies of **C5** and **C9** were comparable at this level (within 1 kJ mol⁻¹), we deemed it the best balance between chemical accuracy and computational cost. To test how shallow the potential energy landscape of cage **1** is, we performed a relaxed potential energy scan for all conformers at fixed acid-acid separations between 7 and 10 Å and identified five low-energy structures (**C5, C9, C10, C12,** and **C13**) within 10 kJ mol⁻¹ (Fig. 2). Those conformers were also the five lowest-energy conformers for each benchmarked functional. No interconversion between different amide configurations was observed for those five structures during the potential energy scan.

Inspired by the conformationally-rich flat potential energy landscape suggested by these calculations, we designed a semi-automated crystallisation protocol to streamline our experimental search for different cage conformations. We first screened the solubility of cage **1** in 37 organic solvents using the commercially-available ChemSpeed SWING ISYNTH platform. Solvents and antisolvents were identified by solid dispensing of **1** (10 mg) and liquid dispensing of solvents (1 ml) into vials, followed by visual assessment of dissolution (for a full list of solvents, see Table S1). We then developed an automated method for rapidly preparing solvent-antisolvent diffusion crystallisation experiments. Stocks of the cage were prepared in the 'good' solvents and then dispensed into vials. The antisolvent was carefully layered on top, and samples were left in a fume hood to crystallise. We adjusted the automatic liquid dispensing conditions to improve layer formation between the solvent and the antisolvent, to slow mixing and improve crystallinity of the resulting material (ESI, Section 1.2). Around 90 crystallisation experiments were prepared over two separate screens using the ChemSpeed platform.

The initial strategy for the crystallisation experiments was to analyse samples by high-throughput powder X-ray diffraction (PXRD) and compare powder patterns to identify clusters of different polymorphs, which could indicate a different cage conformation, before attempting to obtain single crystals of any promising candidates. After two weeks, vials were visually assessed and any samples that appeared suitable for single-crystal analysis were set aside. The remaining samples containing precipitate were dried and analysed by PXRD (ESI, Table S2). In principle, PXRD analysis is more amenable to high-throughput measurements in our setup due to the relative ease of sample preparation and analysis compared to single-crystal diffraction.[34,46] However, the PXRD data obtained from the first crystallisation screen suggested the formation of solvates and also that structural changes occur upon desolvation of cage **1** (ESI, Table S3). Hence, high-throughput assessment of whether samples contain different conformers was not ultimately possible from PXRD analyses alone, and we therefore focused on single-crystal diffraction for subsequent experiments.

All single crystals were examined by optical microscope to determine their morphology, both for samples obtained directly from the crystallisation screens or those grown manually using promising conditions identified by PXRD. Suitable crystals were selected and mounted onto the diffractometer, and their unit cell parameters were determined. Crystals that possessed both a morphology and unit cell that closely matched a previously collected dataset were assumed to have the same crystal structure and were therefore not studied further. Several crystals were not stable to exposure of air. For some of these crystals it was possible to obtain the lattice parameters but not collect a full data set, while for others no data could be collected. The samples for which partial or complete single-crystal data could be collected are summarised in Table S3.

We identified all five of the predicted stable cage conformers (**C5, C9, C10, C12,** and **C13**) among the crystals where we could obtain a full dataset and structure solution. No other conformations were observed in any of the obtained crystal structures. Figure 3 shows the isolated molecules of cage **1** in those conformations extracted from the crystal structures (see ESI for crystallographic details). Furthermore, three new polymorphs of **C9** were also identified.
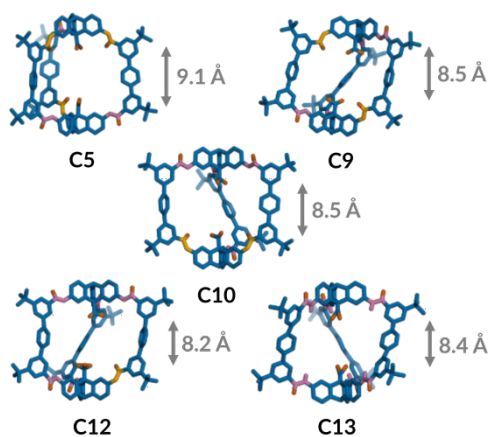
Journal Name

Fig. 3 Five distinct cage **1** conformations found in experimentally obtained crystal structures. The amide carbonyl groups pointing outside the cavity are shown in purple and inside – in orange. Main cage scaffold is shown in blue, oxygen in red. Hydrogen atoms and solvent molecules were removed for clarity. Average observed cavity heights (distances between two acid carbon atoms) are listed alongside the structures.

The most commonly observed conformer was **C9**, which was present in the majority of the collected structures. Despite having the highest predicted energy of the five conformers, **C10** was found in two crystal structures, as a co-crystal with either **C9** or with **C12**. We hypothesise that **C10** can substitute isomorphously for **C9** and **C12** in the extended structures, due to the small difference in cavity height between the three conformers, thus benefitting from the overall stability of the **C9** and **C12** structures. This suggests that crystallisation may be driven at least partially by the pore volume of the cage molecules. Additionally, cage conformations at either extreme of the predicted cavity height range (**C5** and **C13**) are each found in only one crystal structure. The structure containing **C5** has four cage molecules in the unit cell. Three of these molecules are in the **C5** configuration, while the fourth molecule is disordered between **C5** and **C9**. **C5** and **C9** have the largest and second-largest cavity heights, respectively, further suggesting that conformers with similar overall cavity heights may be able to interchange in the extended structures.

Interestingly, **C5** and **C13** were found to crystallise in separate experiments from the same solvent system, perhaps as a result of variations in stock concentration, which was not a factor we investigated during the initial automated screen. We also note that while our approach allowed the rapid identification of the target conformers, rotation of the amide bonds could result in very subtle changes to the unit cell, and hence some interesting polymorphs might have been missed. Clearly, the measurement of single-crystal data is a significant bottleneck to a thorough exploration of solid-state landscapes, which we will tackle in future studies.

Although we do not fully understand what drives the formation of the different conformers, crystallisation appears to be subtly influenced by a combination of factors, as reported previously for organic cages.[32–34] Hirshfeld surface analysis shows that weak π—π and C-H—π interactions dominate the close contacts between molecules in the crystals (Fig. 4 and ESI, Fig. S11). Intermolecular hydrogen bonding between amide groups did not appear to be a major driving force for the crystallisation of one conformer over another. Hydrogen bonding to solvent molecules was observed much more frequently. However, solvent molecules present substantial disorder in all observed diffraction experiments, suggesting that

specific solvent interactions may perhaps not drive the preferential crystallisation in different cage conformers. A representative example of a Hirshfeld surface is shown in Figure 4, highlighting a single strong hydrogen bond between amide groups, and a large number of weaker interactions along the aromatic faces of the triptycene unit.
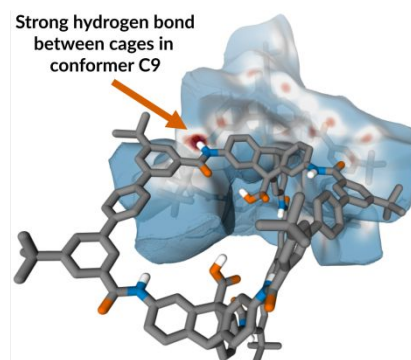

Fig 4 A representative Hirshfeld surface analysis showing hydrogen bonding between two amide groups on neighbouring cage **1** structures in conformer **C9**. Carbon atoms are shown in grey, oxygen in red, nitrogen in blue. Non-polar hydrogen atoms and solvent molecules were removed for clarity.

The **C13** structure, which has no external H-bond donors, is the only crystal system observed here where no hydrogen-bonding occurred between neighbouring cage molecules. In this case, crystal packing was only influenced by weaker van der Waals interactions. Unlike the close-packed arrangement of cage molecules in all other structures, the **C13** molecules pack hexagonally to form 1-D solvent-filled pore channels along the crystallographic **c** axis (Fig. 5). Although porosity was not the focus of this work, this material could in principle exhibit permanent porosity, if the **C13** crystals could be grown on a larger scale and rendered stable to desolvation. The polarity of the carboxylic acid groups in the cage cavity could make this or similar structures interesting from a CO_2 capture perspective.
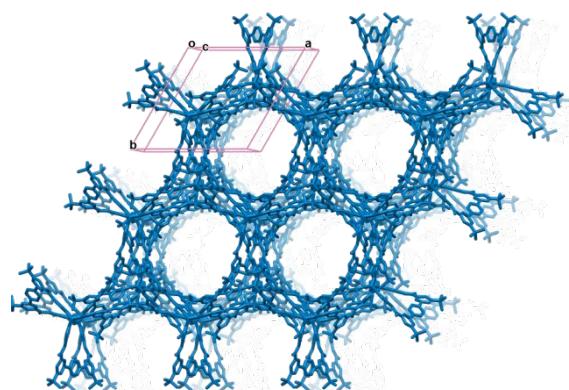

Fig 5 Extended crystal structure of cage **1** in the **C13** conformation, showing hexagonal packing along the crystallographic **c** axis. No hydrogen bonding between neighbouring cages was observed in this structure as all amide carbonyl groups point towards the interior of the cage cavity.

In conclusion, cage **1** shows very flexible behaviour in solution and exhibits different cavity heights corresponding to different relative arrangements of the amide bonds built into the scaffold. The unique cage conformers resulting from these amide bond rotations cannot be resolved on the NMR timescale due to the fast dynamics of the system. Typically, crystallisations of such dynamically evolving

COMMUNICATION   **Journal Name**

mixtures are also a difficult-to-reproduce stochastic process.[47] Here, we demonstrate that it is possible to induce different conformations in the solid state *via* crystallisation. Low-cost computational modelling was used to identify stable conformers of a flexible cage consisting of 250 atoms. These conformers were then realised in different polymorphs using a high-throughput crystallisation workflow using a commercial liquid handling robot that allows for standardisation and reproducibility.[46,48] High-throughput experimentation enables fast and efficient exploration of the vast chemical space and results in FAIR datasets that facilitate future data science and machine learning efforts.[49] Our setup can be directly transferred to any other molecular crystals where it is anticipated that solvent composition can affect crystal formation. A wide range of distances was observed between the two binding groups inside the cage cavity, validating our initial hypothesis that cage **1** can freely interchange between conformers in solution, thus underpinning future studies on binding and catalytic activity of flexible organic cages.

Conflicts of interest

The authors declare no conflicts of interest.

Notes and references

1   S. La Cognata and V. Amendola, *Chem. Commun.*, 2023, **59**, 13668–13678.
2   P. Bhandari and P. S. Mukherjee, *ACS Catal.*, 2023, **13**, 6126–6143.
3   G. Zhang, B. Hua, A. Dey, M. Ghosh, B. A. Moosa and N. M. Khashab, *Acc. Chem. Res.*, 2021, **54**, 155–168.
4   S. Yu, M. Yang, Y. Liu and M. Liu, *Mater. Chem. Front.*, 2023, 7, 3560–3575.
5   K. Jie, Y. Zhou, H. P. Ryan, S. Dai and J. R. Nitschke, *Adv. Mater.*, 2021, **33**, 2005745.
6   X. Yang, Z. Ullah, J. F. Stoddart and C. T. Yavuz, *Chem. Rev.*, 2023, **123**, 4602–4634.
7   D. Hu, J. Zhang and M. Liu, *Chem. Commun.*, 2022, **58**, 11333–11346.
8   T. Kunde, T. Pausch and B. M. Schmidt, *Eur. J. Org. Chem.*, 2021, 2021, 5844–5856.
9   G. Montà-González, F. Sancenón, R. Martínez-Máñez and V. Martí-Centelles, *Chem. Rev.*, 2022, **122**, 13636–13708.
10 V. Leonhardt, S. Fimmel, A.-M. Krause and F. Beuerle, *Chem. Sci.*, 2020, **11**, 8409–8415.
11 E. Ubasart, O. Borodin, C. Fuertes-Espinosa, Y. Xu, C. García-Simón, L. Gómez, J. Juanhuix, F. Gándara, I. Imaz, D. Maspoch, M. von Delius and X. Ribas, *Nat. Chem.*, 2021, **13**, 420–427.
12 D. Chakraborty and P. Sarathi Mukherjee, *Chem. Commun.*, 2022, **58**, 5558–5573.
13 T. Hasell and A. I. Cooper, *Nat. Rev. Mater.*, 2016, **1**, 1–14.
14 M. Liu, M. A. Little, K. E. Jelfs, J. T. A. Jones, M. Schmidtmann, S. Y. Chong, T. Hasell and A. I. Cooper, *J. Am. Chem. Soc.*, 2014, **136**, 7583–7586.
15 T. Kunde, E. Nieland, H. V. Schröder, C. A. Schalley and B. M. Schmidt, *Chem. Commun.*, 2020, **56**, 4761–4764.
16 P. Li, S. Xu, C. Yu, Z.-Y. Li, J. Xu, Z.-M. Li, L. Zou, X. Leng, S. Gao, Z. Liu, X. Liu and S. Zhang, *Angew. Chem. Int. Ed.*, 2020, **59**, 7113–7121.
17 P. Bhandari and P. S. Mukherjee, *Chem. – Eur. J.*, 2022, **28**, e202201901.
18 A. S. Bhat, S. M. Elbert, W.-S. Zhang, F. Rominger, M. Dieckmann, R. R. Schröder and M. Mastalerz, *Angew. Chem. Int. Ed.*, 2019, **58**, 8819–8823.
19 K. G. Andrews and K. E. Christensen, *Chem. – Eur. J.*, 2023, **29**, e202300063.
20 K. G. Andrews, P. N. Horton and S. J. Coles, *Chem. Sci.*, 2024.
21 F. Jia, H. V. Schröder, L.-P. Yang, C. von Essen, S. Sobottka, B. Sarkar, K. Rissanen, W. Jiang and C. A. Schalley, *J. Am. Chem. Soc.*, 2020, **142**, 3306–3310.
22 C. M. Thomas and N. G. White, *Supramol. Chem.*, 1–13.
23 S. Klotzbach and F. Beuerle, *Angew. Chem. Int. Ed.*, 2015, **54**, 10356–10360.
24 L. Zhang, Y. Jin, G.-H. Tao, Y. Gong, Y. Hu, L. He and W. Zhang, *Angew. Chem. Int. Ed.*, 2020, **59**, 20846–20851.
25 E. Berardo, R. L. Greenaway, L. Turcani, B. M. Alston, M. J. Bennison, M. Miklitz, R. Clowes, M. E. Briggs, A. I. Cooper and K. E. Jelfs, *Nanoscale*, 2018, **10**, 22381–22388.
26 V. Abet, F. T. Szczypiński, M. A. Little, V. Santolini, C. D. Jones, R. Evans, C. Wilson, X. Wu, M. F. Thorne, M. J. Bennison, P. Cui, A. I. Cooper, K. E. Jelfs and A. G. Slater, *Angew. Chem. Int. Ed.*, 2020, **59**, 16755–16763.
27 A. G. Slater, M. A. Little, M. E. Briggs, K. E. Jelfs and A. I. Cooper, *Mol. Syst. Eng.*, 2018, **3**, 223–227.
28 B. Chatelet, L. Joucla, J.-P. Dutasta, A. Martinez and V. Dufaud, *Chem. – Eur. J.*, 2014, **20**, 8571–8574.
29 M. W. Schneider, I. M. Oppel, A. Griffin and M. Mastalerz, *Angew. Chem. Int. Ed.*, 2013, **52**, 3611–3615.
30 H.-Y. Chen, M. Gou and J.-B. Wang, *Chem. Commun.*, 2017, **53**, 3524–3526.
31 J. D. Evans, K. E. Jelfs, G. M. Day and C. J. Doonan, *Chem. Soc. Rev.*, 2017, **46**, 3286–3301.
32 W. Wang, K. Su, E.-S. M. El-Sayed, M. Yang and D. Yuan, *ACS Appl. Mater. Interfaces*, 2021, **13**, 24042–24050.
33 D. P. McMahon, A. Stephenson, S. Y. Chong, M. A. Little, J. T. A. Jones, A. I. Cooper and G. M. Day, *Faraday Discuss.*, 2018, **211**, 383–399.
34 P. Cui, D. P. McMahon, P. R. Spackman, B. M. Alston, M. A. Little, G. M. Day and A. I. Cooper, *Chem. Sci.*, 2019, **10**, 9988–9997.
35 P. Pracht, F. Bohle and S. Grimme, *Phys. Chem. Chem. Phys.*, 2020, **22**, 7169–7192.
36 C. Bannwarth, S. Ehlert and S. Grimme, *J. Chem. Theory Comput.*, 2019, **15**, 1652–1671.
37 J. G. Brandenburg, C. Bannwarth, A. Hansen and S. Grimme, *J. Chem. Phys.*, 2018, **148**, 064104.
38 S. Grimme, J. Antony, S. Ehrlich and H. Krieg, *J. Chem. Phys.*, 2010, **132**, 154104.
39 F. Weigend and R. Ahlrichs, *Phys. Chem. Chem. Phys.*, 2005, **7**, 3297–3305.
40 J. P. Perdew, K. Burke and M. Ernzerhof, *Phys. Rev. Lett.*, 1996, **77**, 3865–3868.
41 J. P. Perdew, M. Ernzerhof and K. Burke, *J. Chem. Phys.*, 1996, **105**, 9982–9985.
42 P. J. Stephens, F. J. Devlin, C. F. Chabalowski and M. J. Frisch, *J. Phys. Chem.*, 1994, **98**, 11623–11627.
43 Y. Zhao and D. G. Truhlar, *Theor. Chem. Acc.*, 2008, **120**, 215–241.
44 N. Mardirossian and M. Head-Gordon, *J. Chem. Phys.*, 2016, **144**, 214110.
45 J.-D. Chai and M. Head-Gordon, *Phys. Chem. Chem. Phys.*, 2008, **10**, 6615–6620.
46 A. Lunt, H. Fakhruldeen, G. Pizzuto, L. Longley, A. White, N. Rankin, R. Clowes, B. Alston, L. Gigli, G. Matthew Day, S. Y Chong and A. Cooper, *Chem. Sci.*, 2024, **15**, 2456-2463.
47 E. C. Lee, J. M. Parrilla-Gutierrez, A. Henson, E. K. Brechin and L. Cronin, *Matter*, 2020, **2**, 649–657.
48 R. J. Arruda, P. A. J. Cally, A. Wylie, N. Shah, I. Joel, Z. A. Leff, A. Clark, G. Fountain, L. Neves, J. Kratz, A. A. Thorat, I. Marziano, P. R. Rose, K. P. Girard and G. Capellades, *Cryst. Growth Des.*, 2023, **23**, 3845–3861.
49 M. D. Wilkinson, M. Dumontier, Ij. J. Aalbersberg, G. Appleton, M. Axton, A. Baak, N. Blomberg, J.-W. Boiten, L. B. da Silva Santos, P. E. Bourne, J. Bouwman, A. J. Brookes, T. Clark, M. Crosas, I. Dillo, O. Dumon, S. Edmunds, C. T. Evelo, R. Finkers, A. Gonzalez-Beltran, A. J. G. Gray, P. Groth, C. Goble, J. S. Grethe, J. Heringa, P. A. C. 't Hoen, R. Hooft, T. Kuhn, R. Kok, J. Kok, S. J. Lusher, M. E. Martone, A. Mons, A. L. Packer, B. Persson, P. Rocca-Serra, M. Roos, R. van Schaik, S.-A. Sansone, E. Schultes, T. Sengstag, T. Slater, G. Strawn, M. A. Swertz, M. Thompson, J. van der Lei, E. van Mulligen, J. Velterop, A. Waagmeester, P. Wittenburg, K. Wolstencroft, J. Zhao and B. Mons, *Sci. Data*, 2016, **3**, 160018.

ChemComm Accepted Manuscript